THE JOURNAL OF PHYSICAL CHEMISTRY B

pubs.acs.org/JPCB

Article

Design of Nonideal Eutectic Mixtures Based on Correlations with Molecular Properties

Published as part of The Journal of Physical Chemistry virtual special issue "Deep Eutectic Solvents".

Laura J. B. M. Kollau, Remco Tuinier,* Job Verhaak, Jaap den Doelder, Ivo A. W. Filot, and Mark Vis

Cite This: *J. Phys. Chem. B* 2020, 124, 5209–5219

Read Online

ACCESS | Metrics & More | Article Recommendations | Supporting Information

ABSTRACT: In this work, a statistical analysis was performed to reveal how the molecular properties are correlated with the nonideal behavior observed in eutectic mixtures. From this, a statistical model, combined with theory and experimental results, was developed to predict the nonideal behavior of a specific set of eutectic mixtures, consisting of quaternary ammonium bromides with dicarboxylic acids and polyols. The combination of this analysis and this model can be considered as a first step toward the *a priori* design of eutectic mixtures. The analysis performed is based on principal components. The descriptors used for this are molecular properties of the constituents of these mixtures. The molecular properties are a combination of experimental, theoretical, and computed properties. The analysis reveals that there are strong correlations between the nonideality of the mixtures and a measure of the acidity of the hydrogen bond donating protons, the displacement of the bromide anion, and the bulkiness of the quaternary ammonium salt. Our analysis highlights the design rules of deep eutectic systems (DES), enabling control over the extent of the liquid window. Our model enables prediction of the eutectic temperature for a range of related mixtures.

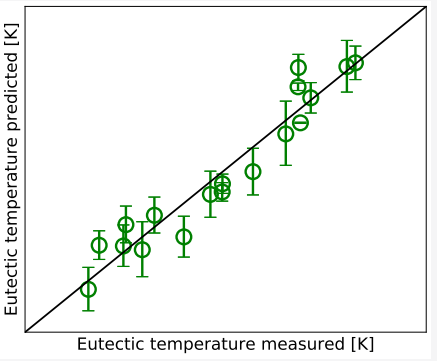

INTRODUCTION

Since the first mentioning of eutectic mixtures as deep eutectic solvents[1] (DESs), they have been compared to ionic liquids (ILs). Ionic liquids are eulogized for being designer solvents. This means that the physical properties of ILs can be tailored based on the choice of the anion and cation. Similar to ILs, DESs have the potential of being designer solvents, tailored toward specific applications based on the choice of the mixture's constituents. However, the understanding of the relation between the molecular properties of DES constituents and the properties of the mixture is still far from complete. Without understanding which properties of the constituents connect to the physical and chemical properties of the mixtures, designer mixtures will not materialize. Research on these relations has until now mostly focused on the dependence of physicochemical properties, such as density and viscosity, on the hydrogen bond donor bonding capacity,[2,3] the water content,[4,5] or temperature.[6,7] Recently, Abranches et al. reported results on similar salt mixtures and observed unexpected nonidealities.[8,9] It is however difficult to draw conclusions from these types of mixtures, as the ideal reference state is unknown due to a lack of fusion property data of the pure compounds. Therefore, this reference state can only be estimated.[10,11] Recently, the importance of differences in acidities was pointed out for the preparation of nonionic, nonideal eutectic mixtures.[12]

García and co-workers aimed at relating the electronic energy, a computed molecular property, of several mixtures to their observed eutectic melting point.[13] Their study is of particular interest when screening new mixtures for applicability in the desired temperature range. However, the method employed still requires the electronic energy to be computed for every *mixture* under consideration. For ILs, progress was made with *a priori* screening for certain properties of not yet synthesized ILs via standardized computed quantities, for example, predictions of the Kamlet–Taft parameters.[14]

In this paper, a step toward *a priori* design of the liquid window of nonideal eutectic mixtures is endeavored. For this, common physical properties and estimations of the molecular interactions obtained via density functional theory (DFT) of the *individual* components were gathered. It is hypothesized that these properties contribute to the attractions between the different components and to be responsible for the nonideal behavior of the eutectic mixtures. These properties were examined using a principal component analysis to identify their

Received: February 26, 2020
Revised: May 29, 2020
Published: June 12, 2020

https://dx.doi.org/10.1021/acs.jpcb.0c01680
J. Phys. Chem. B 2020, 124, 5209–5219

relations to interaction parameters obtained from phase diagrams of 18 systems. Using these relations, the nonideality and thus the eutectic temperatures for the 22 other systems were predicted. With this approach, we developed a first step toward a theoretical framework for the quantification, the description, and the prediction of the phase behavior of DESs.

Thermodynamic Quantification of the Nonideality. The nonideal contributions to the melting point depression can be quantified by obtaining interaction parameters via a description of the molar Gibbs energy g of mixing and by differentiating between contributions from (molar) entropy s and (molar) enthalpy h:

$$g = h - Ts \tag{1}$$

Here g can be related directly to experimentally obtained solid−liquid phase diagrams via the chemical potential μ

$$\left(\frac{\partial ng}{\partial n_i}\right)_{p,T,n_j} = \mu_i - \mu_i^* = RT \ln \gamma_i x_i \tag{2}$$

where n is the total number of moles, n_i is the number of moles of component i, x_i is the mole fraction, and γ_i is the activity coefficient. Here $\mu_i - \mu_i^* = \Delta\mu_i$ is related to the melting point depression of the mixture and to pure component properties through the Schroeder−van Laar equation

$$\frac{\Delta\mu_i}{RT} = \frac{\Delta H_i}{R}\left(\frac{1}{T_i^*} - \frac{1}{T}\right) \tag{3}$$

where ΔH_i is the enthalpy of fusion, T_i^* the melting point of the pure component i, and T the melting point of the mixture.

The entropy model used here is the volume- and surface-based Staverman−Guggenheim entropy with s given by

$$s = x_1 \ln \phi_1 + x_1 Q_1 \ln\left(\frac{\theta_1}{\phi_1}\right) + x_2 \ln \phi_2 + x_2 Q_2 \ln\left(\frac{\theta_2}{\phi_2}\right) \tag{4}$$

Here ϕ denotes the volume fraction, defined by

$$\phi_i(x_i, V_{m,i}) = \frac{x_i V_{m,i}}{\Sigma_i x_i V_{m,i}} \tag{5}$$

and θ represents the surface fraction

$$\theta_i(x_i, A_{m,i}) = \frac{x_i A_{m,i}}{\Sigma_i x_i A_{m,i}} \tag{6}$$

with $V_{m,i}$ and $A_{m,i}$ being, respectively, the molar volume and surface for component i. Here Q_i is a direct function of ϕ_i and θ_i:

$$Q_i = \frac{1 - \frac{\phi_i}{x_i}}{1 - \frac{\phi_i}{\theta_i}} \tag{7}$$

To characterize the enthalpic contributions, regular solution (RS) theory[15,16] is used. RS theory quantifies the enthalpic contributions using one interaction parameter, χ, and was shown to accurately describe nonidealities typically found in DESs:[17]

$$\frac{h}{RT} = \chi x_1 x_2 \tag{8}$$

This expression was first proposed by Margules,[18] without invoking lattice approaches introduced later, which allow the interaction parameter χ to take both positive and negative values, depending on the relative interactions between the components. It should also be stressed that, while for apolar systems the χ parameter may be predicted from (Hansen) solubility parameters, this is not straightforward for polar systems where hydrogen bonding plays a role.[19]

Previously, it was demonstrated that a Redlich−Kister-like expansion can be used to more accurately describe the solid−liquid phase boundaries without changing the value, or physical meaning, of χ due to the orthogonal nature of Legendre polynomials.[20] Therefore, χ can be determined accurately, based only on the fusion properties of both components and the eutectic temperature measured for the mixture using only RS theory.

Combining RS theory and Staverman−Guggenheim[21−24] results in the following expression for $\Delta\mu_i$:

$$\frac{\Delta\mu_i}{RT} = \ln \phi_i - Q_i \ln \frac{\phi_i}{\theta_i} + \chi(1 - x_i)^2 \tag{9}$$

Model Systems. The full set of systems consists of eight hydrogen bond donors (HBDs) and five hydrogen bond acceptors (HBAs), resulting in 40 possible combinations. New DESs were developed rather than using previously published data to ensure that components have well-defined physical properties and do not react with themselves or each other; e.g., combinations of carboxylic acids and alcohols, which can react to esters, were avoided.[25] Since already the selection of compounds that are suitable for determining the phase behavior is not straightforward, we therefore restricted ourselves to these 40 combinations. This selection resulted in the hydrogen bond donors and acceptors shown in Figure 1. These components differ systematically in specific features. For example, for the HBD in the dicarboxylic acid series, ranging from succinic acid to suberic acid, the alkyl chain length increases stepwise by a single carbon atom. This causes the molecule to become slightly less hydrophilic and to adopt

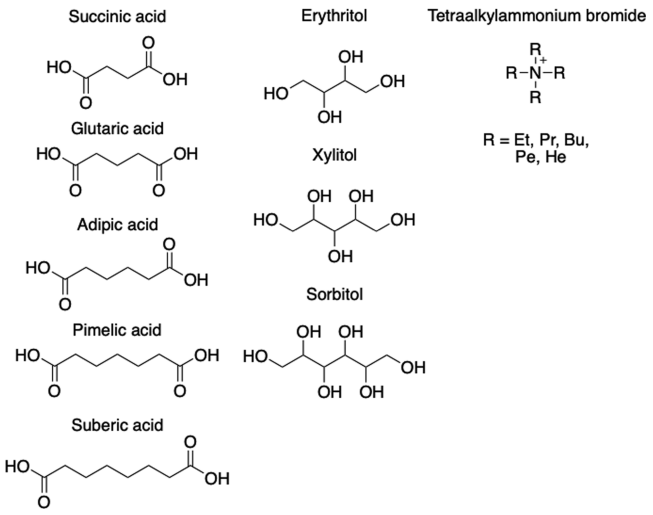

Figure 1. Molecular structures of the individual components of the binary mixtures studied here. The H-bond donating components are displayed individually. The H-bond accepting components are depicted via a general structure, where R represents the alkyl groups ethyl, propyl, butyl, pentyl, and hexyl.

https://dx.doi.org/10.1021/acs.jpcb.0c01680
J. Phys. Chem. B 2020, 124, 5209−5219

Table 1. Experimentally Obtained Melting Point T, Enthalpy of Fusion ΔH, Molar Volume V_m, and Molecular Surface A_m of the Individual Components of the Binary Mixtures Studied as well as the Literature Values (ref) of Several Compounds

	T (K)		ΔH (kJ·mol^{-1})			
component	meas.	lit. (ref.)	meas.	lit. (ref.)	V_m[b] (cm^3·mol^{-1})	A_m[b] (cm^2·mol^{-1})
succinic acid	460.0	457.1 (28)	37.1	32.6 (28)	41.9	10.6
glutaric acid	371.6	371.0 (28)	21.5	20.9 (28)	52.2	13.1
adipic acid	426.2	426.4 (28)	37.4	34.9 (28)	62.2	15.5
pimelic acid	378.5	377.5 (28)	26.1	27.6 (28)	66.5	16.5
suberic acid	415.3	417.3 (28)	30.2	28.8 (28)	75.4	18.6
erythritol	394.7	365.9 (29)	39.3	36.5 (29)	46.4	11.7
xylitol	370.4	391.9 (29)	36.6	40.7 (29)	55.6	13.9
sorbitol	369.6	366.4 (29)	22.5	27.7 (29)	66.9	16.6
Et_4NBr	633[a]		13.9[a]		83.3	20.5
Pr_4NBr	563[a]		7.8[a]		121.6	29.7
Bu_4NBr	390.8	395.2 (30)	10.0	15.5 (30)	150.0	36.5
Pe_4NBr	375.9	376.2 (30)	40.1	41.4 (30)	190.7	46.2
He_4NBr	370.6	377.2 (30)	11.6	15.9 (30)	220.0	53.2

[a]Estimated from solid−liquid equilibrium data.[31] [b]Generated by MolModPro software.

more conformations to alternate between cis and trans. This alternation for the odd and even dicarbolyxic acids is known to influence the melting point and enthalpy of fusion.[26,27] The polyols used range from erythritol to sorbitol, also increasing in chain length, but here the number of hydroxyl groups increases simultaneously. The alkylammonium bromides (HBAs) range from tetraethyl- to tetrahexylammonium bromide, which we will refer to as Et_4NBr, Pr_4NBr, Bu_4NBr, Pe_4NBr, and He_4NBr.

Table 1 shows the fusion properties, molar volume, and molecular surface for the considered components measured by us and compared to literature values. The values obtained for the components used for this work are in most cases in good agreement with the literature values. The fusion properties for Et_4NBr and Pr_4NBr could not be obtained experimentally, as these salts degrade before melting. For these components, an alternate procedure has been adopted. For these systems, the liquidus curves for the mixtures were measured at molar ratios accessible by our techniques. The data points, of all mixtures containing the salt of interest, were then simultaneously fitted to eq 9, from which the unknown fusion properties were derived as global fit parameters for all mixtures and χ as an individual fit parameter for each mixture.

Table 2 lists the obtained eutectic temperatures and interaction parameters χ for the mixtures considered. All of the phase diagrams obtained for this work are presented in Figures S1−S3. When comparing the interaction parameters for the different mixtures, a few trends can be observed. For example, binary mixtures of adipic acid with three different quaternary ammonium salts were analyzed, in which χ becomes less negative with increasing length of the side chains of these salts, indicating stronger attraction with smaller quaternary ammonium salt. This might suggest that the bromide anion is more accessible when the side chains are shorter. However, this trend does not extend to succinic acid, of which also binary mixtures were studied with three salts. Here Pe_4NBr shows a larger negative deviation than Bu_4NBr.

Another observation from the interaction parameters from these mixtures comes from the mixtures with Et_4NBr as HBA. Here the interaction parameter becomes more negative with decreasing molecular size, while it follows the odd−even effect described earlier for these dicarboxylic acids. This effect explains why χ for adipic acid with Et_4NBr is slightly more negative then one would expect and very close to the χ obtained for glutaric acid with Et_4NBr. When considering these trends, an oddity is observed in the mixture of pimelic acid with Pe_4NBr. As pimelic acid is larger than succinic acid, it would be expected to have a χ closer to zero than succinic acid with Pe_4NBr. Looking further into the trend of pimelic acid with the different quaternary ammonium salts, again an oddity is observed. Also, here the previously observed trend of stronger interactions with smaller cations is broken.

Table 2. Measured Eutectic Temperatures T_e and Extracted Interaction Parameters χ of the Eutectic Mixtures Studied with Hydrogen Bond Donors and Acceptors Indicated

HBD	HBA	T_e (K)	χ
succinic acid	Et_4NBr	352.6	−7.92
adipic acid	Et_4NBr	352.5	−5.53
glutaric acid	Et_4NBr	303.3	−5.44
erythritol	Et_4NBr	346.1	−4.79
pimelic acid	Et_4NBr	323.5	−4.29
adipic acid	Pr_4NBr	344.9	−3.67
pimelic acid	Pr_4NBr	321.0	−2.26
sorbitol	Pr_4NBr	336.3	−0.64
suberic acid	Bu_4NBr	315.9	−3.15
xylitol	Bu_4NBr	313.2	−2.24
succinic acid	Bu_4NBr	355.8	−1.30
sorbitol	Bu_4NBr	312.5	−1.03
pimelic acid	Pe_4NBr	309.6	−5.95
succinic acid	Pe_4NBr	349.3	−4.01
sorbitol	Pe_4NBr	319.7	−3.43
xylitol	Pe_4NBr	332.4	−2.77
erythritol	Pe_4NBr	346.4	−1.90
adipic acid	He_4NBr	332.0	−2.16

Properties as Descriptors. Trends in nonideality in eutectic mixtures observed in earlier publications[17,20] suggest a relation with hydrogen bonding, where nonideality is supposed to increase with stronger hydrogen bonds. However, no straightforward and general rule of thumb is yet established to support such a relationship, as discussed in the previous section. Here, it is hypothesized that the nonideality of mixtures can be qualitatively predicted based on their corresponding H-bond characteristics. Achieving these predictions will result in a better understanding of the interactions

https://dx.doi.org/10.1021/acs.jpcb.0c01680
J. Phys. Chem. B 2020, 124, 5209−5219

responsible for the dramatic melting depressions from which deep eutectics gained their names.

In order to include a wide range of properties in this exploration, common and new properties of the individual components were used. The properties chosen are expected to indicate the strength of the H-bond interactions, such as pK_a, molecular dipole moments, and number of H-bonding moieties. Furthermore, H_2O solubility as well as the Hansen solubility parameters of the components of the binary mixtures were considered. Quantitative information on hydrogen bonds can also be computed,[32] for example, by using density functional theory.

These properties will be used as descriptors in a principal component analysis and for a regression analysis. The goal is to identify which properties, or combination of properties, can explain the trends in nonideality, as observed in a selected set of eutectic mixtures, which later also will be used to predict eutectic properties of the mixtures.

Properties. It can be rationalized that all properties used are candidates for explaining the variety in nonideality, quantified as interaction parameters, observed in the eutectic mixtures studied here. Logically, the fusion properties, the enthalpy of fusion ΔH and melting point T^*, are already considered as part of the entropy of fusion and may not contribute to the enthalpy of mixing. However, a synergistic effect between the fusion properties and another property should not be excluded from the correlations.

Hydrogen bonds are directly related to the Brønsted acidity of components.[35,36] Hence, the acid dissociation constant K_a, expressed as pK_a, is added as a descriptor to quantify the hydrogen bond capabilities. The proton affinity[37] is closely related to the pK_a and is calculated here using DFT, as described in the Methods section. Next to the proton affinity, the solubility of the components in H_2O as well as their molecular dipole moments were used as descriptors. The dipole moments again show the odd/even behavior for the dicarboxylic acids. These properties are listed in the Supporting Information, Table S3. The enthalpic interactions expected to be responsible for the observed nonideality will not only depend on the hydrogen bond capable moiety but also depend on the rest of the molecule. It is observed in the trends of Table 2 that smaller dicarboxylic acids usually result in stronger attractions.

Similarly, for the quaternary ammonium bromides, longer side chains could make them less accessible, as the interactions are assumed to be taking place through the bromide anion. It is also expected that the amount of hydrogen bond capable groups will influence the nonideal behavior in the mixtures. A selection of these parameters is presented in Table 3. The complete set of parameters can be found in the Supporting Information.

The Hansen solubility parameters are based on the "like dissolves like" concept and are partial solubility parameters which differentiate between dispersive forces, polarity, and hydrogen bonding ability. The Hansen solubility parameters,[38] listed in the Supporting Information (Table S4), were estimated using a group contribution method.[39]

Other interesting features may result from interactions of the component of interest with a probe molecule. Their difference in behavior toward the same molecule may yield insight into their behavior in mixtures with each other. To obtain these interactions, density functional theory (DFT) computations were used. Details on the calculations are described in the

Table 3. Physical Properties of the Individual Components Related to the Molecular Structures: the Molecular Mass M, Density of the Solid Crystalline Components ρ, and Number (#) of $-CH_2$ Groups[a]

component	M ($g \cdot mol^{-1}$)	ρ[b] ($g \cdot cm^{-3}$)	# of $-CH_2$	proton affinity (eV)	molecular dipole moment (D)
succinic acid	118.09	1.56	2	1.159	2.14[33]
glutaric acid	132.12	1.402	3	1.448	2.37[33]
adipic acid	152.1	1.355	4	1.513	2.30[33]
pimelic acid	160.17	1.335	5	1.619	2.36[33]
suberic acid	174.2	1.28	6	1.71	2.34[33]
erythritol	122.12	1.459	0	1.41	3.20[34]
xylitol	152.15	1.516	0	1.745	3.60[34]
sorbitol	182.17	1.509	0	1.578	3.90[34]
Et_4NBr	210.16	1.397	4	1.218	
PR_4NBr	266.26	1.213	8	1.213	
Bu_4NBr	322.37	1.191	12	1.127	
Pe_4NBr	378.47	1.100	16	1.204	
He_4NBr	434.59	1.094	20	1.206	

[a]Properties of the individual components related to the acidity of the hydrogen bonding moieties: the proton affinity (PA) and the molecular dipole moment. [b]Experimentally obtained using a Micromeritics AccuPyc II 1340 Gas pycnometer.

Methods section. The obtained properties from these calculations are the ground state energies and the optimized distance between the oxygen atom and proton in the −OH groups used to form the hydrogen bond. These properties are calculated for the isolated molecules and in the presence of another probe molecule. Water and formic acid were taken as probe molecules. These probe molecules were chosen for their small size and dual nature of being both donors as well as acceptors of hydrogen bonds. For the acceptors, the optimized distance between the oxygen and the proton in the probe molecule was calculated additionally. Figure 2 presents an overview of the situations considered for the computed properties. The labels are the notations used to refer to specific distances in the molecules. The quantity h refers to a distance between an oxygen atom and a proton. The variable b is used to denote the distance between the N^+ cation and Br^- anion. The sub- and superscripts refer to the molecule considered and the molecule inducing an interaction, respectively. For example, h_i^{FA} refers to the distance between the oxygen atom and the proton in component i while it interacts with formic acid. The annotations of the differences in ground state energies of the molecules are defined in Figure 2 and Table 4. Here the sub- and superscripts refer to the final ground state and the initial ground state(s), respectively.

The resulting ground state energies ΔE are listed in the Supporting Information (Table S5) for all studied components. The optimized distances of each component i, h_i and b_i, in the different environments are listed in the Supporting Information (Tables S6 and S7).

Principal Component Analysis. In order to thoroughly evaluate the variety of and correlations between the properties discussed, a principal component analysis (PCA) is performed. The goal of this PCA is to extract information from the data and to express this information as a set of new orthogonal variables called principal components (PCs). These PCs are

https://dx.doi.org/10.1021/acs.jpcb.0c01680
J. Phys. Chem. B 2020, 124, 5209−5219

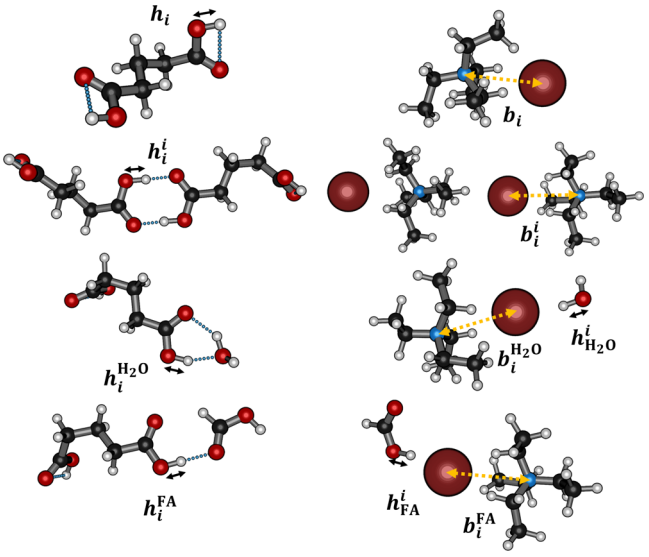

Figure 2. Visualization of the characteristic distances obtained from DFT calculations; h_i denotes the distance between an oxygen atom and a proton, indicated by black arrows; b_i represents the distance between the N^+ cation and Br^- anion, indicated by the dotted yellow arrows. The subscripts refer to the central molecule; the superscripts refer to the molecule inducing intermolecular interactions.

Table 4. Properties Resulting from the Differences in Electronic Energy with the Probe Molecules Calculated via ΔE = Electronic Energy of the Final State − Electronic Energy of the Initial State 1 − Electronic Energy of the Initial State 2 for Component *i*

final ground state energy	initial ground state energy 1	initial ground state energy 2	abbreviation
$2i$	i	i	ΔE_{2i}^i
$i + H_2O$	i	H_2O	$\Delta E_{H_2O}^i$
i + FA	i	FA	ΔE_{FA}^i
ΔE_{2i}^i	$\Delta E_{H_2O}^i$		$\Delta E_{2i}^{H_2O}$
ΔE_{2i}^i	ΔE_{FA}^i		ΔE_{2i}^{FA}

obtained as linear combinations of the original variables and reduce the dimensionality of the data set by keeping only the most distinguishing information.[40,41] The first principal component is the linear combination of the variables that shows the largest variance. The second principal component is the combination that gives the largest variance while orthogonal to PC1.

Since the eutectic mixtures are combinations of the hydrogen bond donors and the quaternary ammonium salts, every mixture will be characterized by 48 descriptors, 25 of the hydrogen bond donor and 23 of the hydrogen bond acceptor; see the Supporting Information (Tables S9 and S10). These 48 variables will be reduced to principal components (PCs). The eigenvalues of the principal components, of which the total sum equals unity, indicate the contribution of the respective PC to the variation in the data. Table 5 lists the eigenvalues of the first six principal components. These eigenvalues show that PC1 and PC2 contribute equally while the eigenvalues decrease from PC3 and further on. The sum of the eigenvalues reveals that the first four principal components can account for about 80% of the variation in the data and the first six for about

Table 5. Eigenvalues of the First Six Principal Components, PC1, PC2, PC3, PC4, PC5, and PC6

principal component	eigenvalues	cumulative eigenvalues	donor or acceptor
PC1	0.315	0.315	acceptor
PC2	0.311	0.626	donor
PC3	0.093	0.719	donor
PC4	0.074	0.793	acceptor
PC5	0.054	0.847	acceptor
PC6	0.048	0.895	donor

90%. However, in order to minimize the number of free parameters, only the first four PCs will be considered further.

The so-called scores of the mixtures are the new coordinates describing the mixtures generated by the PCs. By plotting these scores for all mixtures, one can visualize whether the PCs are able to distinguish the mixtures, as the goal of the PCA is to generate unique coordinates for each mixture. The first four principal components are plotted in Figure 3. Here every

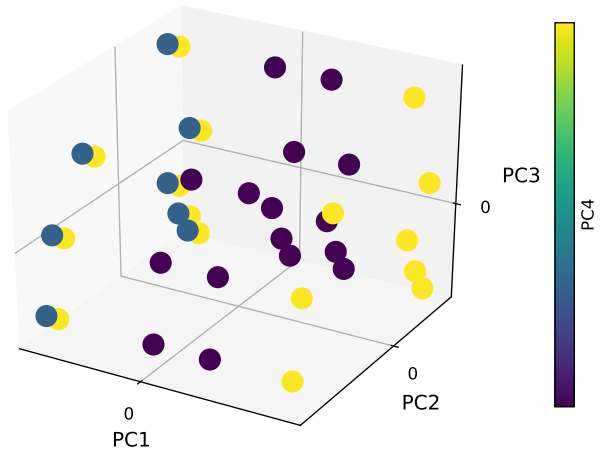

Figure 3. Score plot of the first four principal components of the eutectic mixtures.

marker represents a mixture with a specific acceptor and a specific donor. It is evident that the mixtures are well separated in this representation. The coordinates for each specific mixture can be found in the Supporting Information, Table S8.

The principal components describe either the hydrogen bond donating component or the hydrogen bond accepting component, since the properties we use of HBD and HBA are independent. The properties were not divided beforehand. For this reason, it is evident that the principal components are to be used in pairs, both accounting for the accepting components as their donating counterparts. This is also intuitive from a physical−chemical point of view.

Next to generating unique coordinates for all mixtures, the principal components contain information about the significance of the variables used. The eigenvectors of the principal components, usually referred to as the loadings, directly describe the composition of the PC by the variables and can be visualized in a loadings plot. The loadings plot of PC1 and PC4, both describing the hydrogen bond acceptors, is presented in Figure 4 (left panel). Variables with similar loadings in the PCs are highly correlated or contain similar information. The length of these vectors represents their contribution to the principal component. Analyzing the

https://dx.doi.org/10.1021/acs.jpcb.0c01680
J. Phys. Chem. B 2020, 124, 5209−5219

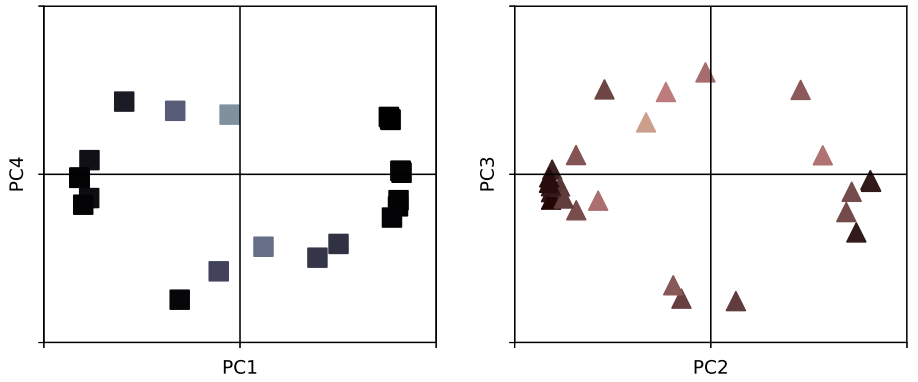

Figure 4. Loadings plots of the descriptors contributions to the principal components. Colors indicate the distance to the origin, where lighter is closer to the origin.

loadings plot of PC1 and PC4, two main clusters can be observed. These clusters contain variables which are closely related to each other and contain more or less the same information. Similar clusters are observed in PC2 and PC3; however, here the right cluster is less dense, thus containing less variables.

The distances of the loadings to the origin, which indicate their contribution to the principal components, are listed in Table 6. The distances are determined using the two most important PCs per category.

RESULTS AND DISCUSSION

What can be noted directly from the loadings of the descriptors of the donors in Table 6 in the left column is that the dipole moment, the Hansen solubility parameters δH and δP, and the number of −COH groups in the molecule are highly related and contribute most to the variation observed in the donors. It is not surprising that these properties are highly related, as the dipole moment strongly depends on the different moieties related to hydrogen bonding. Also, the Hansen solubility parameters δH and δP describe the hydrogen bonding ability and the polarity of a molecule. This cluster of properties is closely followed by the remaining structure descriptors, being # of CO, # of CH_2, the bond length between the oxygen and the proton of the acid group when interacting with itself h_i^i, and δD. Also, here the findings are according to expectations. It is well-known that the availability of a proton for hydrogen bonding depends not only on the direct neighbors but also on the entire molecular structure for such small molecules. Descending with the length of the vectors means that these properties do not contribute as much to the variety in the information provided for these components. The lowest contributing properties for the HBD are the fusion properties, as here the lengths suddenly drop significantly, and several computed properties related to the probe molecules.

Table 6. Loadings of the Principal Components[a]

descriptor donors	length	descriptor acceptors	length
dipole moment	0.993	ΔE_{2i}^{FA}	1.000
δH	0.992	ΔE_{2i}^{i}	0.999
δP	0.989	$\Delta E_{2i}^{H_2O}$	0.998
# of −COH	0.986	b_i	0.993
# of $-CH_2$	0.982	V_m	0.988
h_i^i	0.982	$b_i^{H_2O}$	0.987
δD	0.981	ρ	0.983
# of =CO	0.977	δD	0.982
pK_a	0.971	δH	0.982
ΔE_{2i}^{i}	0.926	# of $-CH_2$	0.982
V_m	0.917	δP	0.982
ΔE_{2i}^{FA}	0.915	M	0.982
M	0.905	b_i^{FA}	0.979
ρ	0.889	b_i^{i}	0.967
h_i	0.872	T^*	0.938
$h_i^{H_2O}$	0.871	h_{FA}^{i}	0.926
H_2O solubility	0.862	H_2O solubility	0.878
$\Delta E_i^{H_2O}$	0.836	ΔS	0.781
proton affinity	0.824	ΔH	0.760
T^*	0.815	proton affinity	0.704
ΔH	0.728	$h_i^{H_2O}$	0.602
$\Delta E_{2i}^{H_2O}$	0.714	$\Delta E_i^{H_2O}$	0.536
h_i^{FA}	0.698	ΔE_i^{FA}	0.430
ΔS	0.649		
ΔE_i^{FA}	0.543		

[a]The values of the loadings are the distance to the origin and are determined using the two most important PCs per category.

For the loadings of the acceptors, in Table 6 in the right column, a similar grouping of descriptor clusters can be observed. Here the electronic energy differences with the probe molecules and two identical molecules all contribute highly. It is somewhat surprising that the response to the probe molecule compared to the self-interaction and an identical molecule all contain the same information, making the use any of the probe molecules here good candidates for testing interaction abilities of quaternary ammonium salts. Another interesting observation is the apparent difference in information provided by the bromide anion distance between the anion and the cation, b_i, and the length of the side chains of the cation. These quantities were expected to be highly related, as longer side chains are assumed to make the charged cation less accessible. Again, here the fusion properties score very low as contributors. Together with the proton affinity and the reaction of a single molecule to a probe molecule, they contribute least.

Based on these results, a selection was made of the properties which contribute most to the variation of the data, and are not highly correlated. These properties are listed in Table 7 and are used to develop a statistical model to predict the nonideality of the remaining mixtures which were not measured in this work.

https://dx.doi.org/10.1021/acs.jpcb.0c01680
J. Phys. Chem. B 2020, 124, 5209−5219

Table 7. Descriptors of Both Donors and Acceptors Used for the Regression and Their Aliases

descriptor	donor/acceptor	symbol
ΔE_{2i}^{FA} (eV)	acceptor	A_1
b_i (Å)	acceptor	A_2
ρ (g·cm^{-3})	acceptor	A_3
# of $-CH_2$	acceptor	A_4
δH	acceptor	A_5
dipole moment (D)	donor	D_1
# of −COH	donor	D_2
ΔE_{2i}^{FA} (eV)	donor	D_3
ρ (g·cm^{-3})	donor	D_4
proton affinity (eV)	donor	D_5

One may question why the solid phase density could be a fundamental descriptor for both hydrogen bond donors and acceptors. The density gives information on how well molecules are packed into lattices. The packing of crystal lattices has a great influence on the melting properties. This should not affect the nonideality of course, but it does influence the melting temperatures. Indeed, we do see more deviations from nonideality when glutaric acid and pimelic acid (the less densely packed ones) are involved, so one could postulate about how this relates to the interactions in the liquid phase due the stereochemistry of the molecule. Perhaps the density is a good indicator of this.

Regression Analysis. Regression was performed to correlate the differences in nonideal behavior observed in the eutectic mixtures and quantified by the interaction parameter χ, as listed in Table 2. The principal component analysis resulted in four principal components, which together account for 80% of the variation in the data. These principal components were used for multiple linear regression, and subsequently to identify the most important properties to use as descriptors. Table 7 lists the descriptors used for the regression and their aliases.

The regression was carried out using JMP software. This software was used for the principal component analysis, for the visualization of results, and for the regression analysis, leading to the various modeling strategies described below.

Models. The regression was performed for various situations: linear regression with the principal components, linear regression with descriptors directly chosen from the physical properties, and a nonlinear version of the latter regression analysis. These descriptors were chosen based on the loadings resulting from the principal components analysis. The results are listed in Table 8. The principal component regression resulted in a model with a correlation coefficient of $R^2 = 0.69$.

The second method of modeling employs the separate dominant donor and acceptor individual descriptors. They are selected based on the PCs. The subsequent models are independent from those based on PCA, and resulting R^2 values can either be poorer or better, depending on the number of allowed terms. Interestingly, the linear model with singular descriptors resulted in a model with a similar accuracy of $R^2 = 0.73$. This means that using a combination of all of the descriptors, in the form of four principal components, does not yield a better description. The reason is that the principle component analysis extracts the greatest variance in the data, but there is no guarantee that this variance will correlate strongly to another quantity (in this case the interaction parameter χ). Therefore, even when using only three singular descriptors, two for the acceptor and one for the donor, a slightly better description is obtained. The descriptors used here are the distance between cation and anion b_i, the Hansen solubility parameter δH which is related to the hydrogen bonding of the acceptor, and the dipole moment of the donor.

Table 8. Descriptors Used for the Regression[a]

	descriptors			
regression	linear terms	quadratic terms	cross terms	R^2
linear	PC1			0.69
	PC2			
	PC4			
nonlinear	PC2	PC4		0.71
	PC4			
linear	A_2			0.73
	A_5			
	D_1			
nonlinear	A_2	D_1	$D_5 \cdot A_4$	0.93
	A_4	A_2	$D_5 \cdot A_2$	
	D_1			
	D_5			

[a]The last column lists the correlation coefficients.

Both linear models can already be considered as statistically relevant; however, the nonlinear model with singular descriptors is significantly better with $R^2 = 0.93$. The fact that the nonlinear model provides a more accurate description suggests the importance of synergistic effects. The prediction of the interaction parameter χ and the subsequently calculated eutectic temperature T_e and eutectic composition x_e of the remaining 22 combinations of the hydrogen bond donors and acceptors, using the model equation (eq S1) presented in the Supporting Information, can be found in Table S2, based on this nonlinear model.

The accuracy of the model is visualized in Figure 5, where the predicted values of the interaction parameter χ and the subsequently resulting eutectic temperature T_e and eutectic composition x_e are plotted versus their experimentally obtained counterparts. The data show close agreement between predictions and observations.

CONCLUDING REMARKS

In this work, the nonideal behavior of 18 eutectic mixtures based on 5 hydrogen bond acceptors and 8 hydrogen bond donors was quantified in terms of the interaction parameter χ from regular solution theory with experimentally determined phase diagrams. For the 22 other possible combinations of acceptor and donor, the nonideal behavior was subsequently predicted using a statistical model developed using the measured 18 mixtures. The theoretical approach used also allowed estimation of the fusion properties of two quaternary ammonium salts which decompose before melting.

In order to model the trends observed in these 18 interaction parameters, a principal component analysis (PCA) was performed on 48 descriptors quantifying various properties, including the hydrogen bonding capabilities, of the components in the mixtures. This resulted in four principal components which were used to identify the relevant properties to perform regression with the interaction parameters.

From the correlations of the variables with the interaction parameter χ, it follows that the bonding strength of the acidic

https://dx.doi.org/10.1021/acs.jpcb.0c01680
J. Phys. Chem. B 2020, 124, 5209−5219

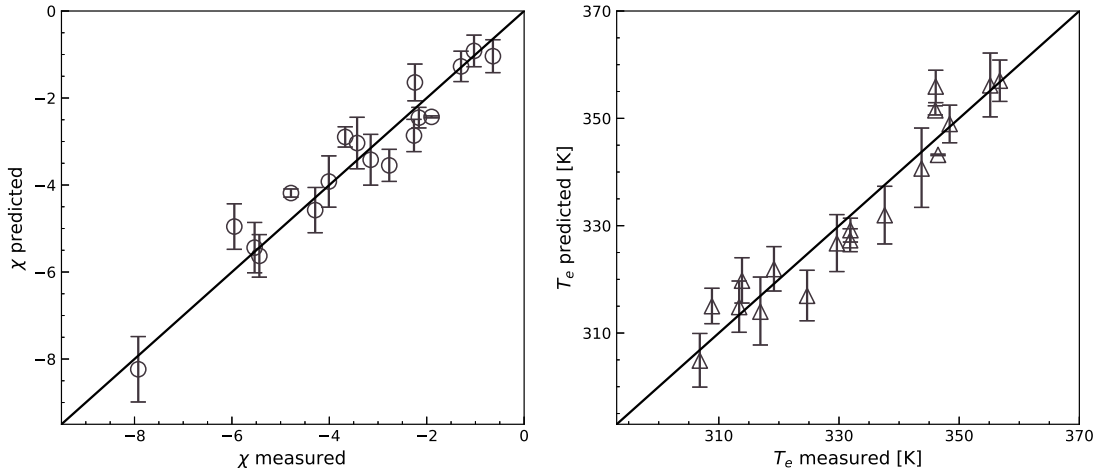

Figure 5. Comparison of the nonideality parameter χ and the eutectic temperature T_e as predicted by the nonlinear model and the measured values.

proton of the hydrogen bond donating groups is important, where a larger dipole moment seems to indicate larger attraction. This bonding strength is measured by the proton affinity and the dipole moment. For the proton affinity, the effect is not as straightforward. In the case of the hydrogen bond acceptor, it shows that the ionic bond length between the bromide anion and the ammonium cation is an important indicator for interactions. Here it seems that a smaller ionic bond leads to stronger attractions; however, this trend is not observed in all cases. Next to this, it follows that the length of the aliphatic side chains of the quaternary ammonium salts is of high importance; also, here the trend is intuitive but again does not apply everywhere. One way to explain these observations is that, due to the shorter side chains, the distance between N^+ and Br^- decreases, and the Br^- anion will experience a larger effective attraction with the −OH of the carboxylic acid or the polyol as compared to itself, which is in agreement with the literature.[8]

From the properties which are present in the model, some generalizations can be made, since these could be regarded as contributors to the enthalpy of mixing. However, as the model comprises nonlinearities, the exact nature of the effect of the properties cannot be derived from this. What is remarkable is that for each donor and acceptor two descriptors are present in the model. The descriptors used for the acceptor here are the distance between the anion and cation of the hydrogen bond acceptor and the length of the aliphatic side chain, thus providing information about the degree of hydrophilicity as well as the bulkiness. For the hydrogen bond donor, both the dipole moment as well as the proton affinity, both being well-known indicators for hydrogen bond donating abilities, are of importance to consider when looking for new nonideal eutectic mixtures. The fact that both HBAs and HBDs are represented in the model does indicate that the nonideality observed in these eutectic mixtures can not easily be ascribed to single properties of the components, for example, to the hydrogen bond donating or accepting ability of the components. It is more likely that the obtained liquid mixtures are the result of a synergistic combination of the properties identified here.

METHODS

Experimental Methods. *Determination of the Eutectic Temperature and Liquidus Curve.* The eutectic temperatures of the different mixtures were measured using melting point capillaries. The DES compositions used were prepared inside a glovebox with a dry nitrogen atmosphere, yielding DES mixtures with moisture levels below 10 ppm. The temperature of the first liquid visible at a heating rate of 5 K·min^{-1} was taken for the solidus line (eutectic temperature). The liquidus curve was (if obtained) measured using DSC on the acid-rich side and using the cloud-point method on the salt-rich side.

DSC Method. A TA Q2000 Dynamic Scanning Calorimeter (DSC) was used to determine ΔH. This equipment has an accuracy of ±0.1 K for T and <1% for ΔH and a precision for T measured of ±0.4 K. Samples were measured in Tzero aluminum hermetic pans. All samples were prepared and pressed inside the glovebox using the mixtures prepared as described in the previous sections. The melting point was obtained by measuring samples of various compositions at three different heating rates (dT/dt), 10, 5, and 1 K·min^{-1}. Prior to every heating cycle, the sample was heated isothermally for at least 10 min at 288 K in order to avoid any metastable intermediate phases.

Cloud-Point Method. A sample was prepared by mixing a known amount of both individual components in a glass vial using a magnetic stirring bar at a certain temperature. The sample was heated in an aluminum heating block, while stirring at 250 rpm, on an IKA RCT basic hot plate with an ETS D-5 temperature controller (accuracy ±0.5 K, precision 0.1 K). The temperature sensor used to control the temperature of the aluminum heating block was immersed in a stirred glass vial with glycerol placed in the aluminum heating block.

At the first chosen temperature, it was evaluated whether enough liquid had formed in order to sample only liquid. Prior to sampling, stirring was turned off and left off for at least 1 h to allow the solids remaining in the vial to settle. Sampling was performed with a micropipette, and care was taken to only sample liquid. After this, the temperature was raised in steps of approximately 4 K until 398 K, or until the melting point of the pure component has been reached, and the sampling procedure was repeated for each step.

The composition of the samples were analyzed using ^{1}H NMR spectroscopy. For this, the samples were dissolved in approximately 1 mL of D_2O (Cambridge Isotope Laboratories Inc., deuterium oxide 99.9%, DLM-4-100, CAS 7789-20-0). Measurements were carried out in 5 mm thin-walled Wilmad

https://dx.doi.org/10.1021/acs.jpcb.0c01680
J. Phys. Chem. B 2020, 124, 5209−5219

NMR tubes using a Bruker BZH 400/52 spectrometer equipped with an autosampler carousel. The spectra were autoshimmed and autophased and recorded in 16 scans with a relaxation time of 5 s by the TopSpin software. The obtained spectra were edited by applying a Withaker Smoother baseline correction and autophase correction using MestReNova 12.0.0-20080.

In order to determine the composition of the sample, the peaks corresponding to specific groups from both components were integrated and normalized to the amount of protons represented by the first peak appearing on the spectrum on the left.

Computational Methods (DFT). All calculations were performed using the Vienna *ab initio* simulation package (VASP).[42−45] The Perdew−Burke−Ernzerhof exchange-correlation functional was used.[46] For the plane wave basis set, a cutoff energy of 400 eV was chosen. All molecules were placed at the center of a sufficiently large unit cell in such a way that the vacuum distance between the compounds in the neighboring super cells was at least 15 Å. It was carefully checked that the charge density approached zero at the border of the unit cell. For all calculations, only the gamma point was employed. Structure optimization was done using the conjugate-gradient algorithm as implemented in VASP. It was verified that after structure optimization the forces on the atoms were less than 0.02 eV/Å in any Cartesian coordinate. Subsequently, ground state energies as well as all of the distances between the available protons and their oxygen for the donors, and cation to anion distances for acceptors, were extracted using a Python script as available within the Atomic Simulation Environment (ASE) package. After the geometry optimization, the probe molecule was added. The probe molecule was either another molecule of the same component or a different molecule, namely, water or formic acid. The positioning of the probe molecule was done identically for all components: The accepting oxygen atom was placed 1.5 Å in front of the donor hydrogen. For HBAs, the donating hydrogen was positioned 2.5 Å from the accepting halide ion. After positioning, another geometry optimization was performed at the same level of theory and using the same methodology as described above. Proton affinities were calculated as the difference in the electronic energy between the components with and without a proton. For the donors, this was achieved by removing a proton from the optimized molecule while keeping the number of valence electrons the same. For the acceptors, a slightly different approach was taken. Since the quaternary ammonium salts do not have a free proton to remove and since the assumption was made that the hydrogen bonding takes place via the bromide anion, a proton was placed at 1.2 Å from the bromide anion in line with the nitrogen cation. To avoid reorganization of the alkyl side chains of the cation, the atoms corresponding to the alkyl side chain were frozen, whereas all other atoms remained unconstrained.

■ ASSOCIATED CONTENT

Supporting Information

The Supporting Information is available free of charge at https://pubs.acs.org/doi/10.1021/acs.jpcb.0c01680.

Final model equation; tables showing parameters for eq S1, predicted and measured eutectic fusion properties of the mixtures, physical properties of the individual components related to the molecular structures, Hansen solubility parameters of the components used, DFT computed properties of the components, computed optimized distances of the components from DFT, listed scores of the first six principal components of the variables, loadings of the principal components 1 and 4 corresponding to the hydrogen bond acceptors, and loadings of the principal components 2 and 3 corresponding to the hydrogen bond donors; and figures showing phase diagrams of binary mixtures of Et_4NBr with succinic acid, glutaric acid, adipic acid, and pimelic acid used to estimate the fusion properties of Et_4NBr, phase diagrams of binary mixtures of Pr_4NBr with adipic acid and pimelic acid used to estimate the fusion properties of Pr_4NBr, and predicted phase diagrams of selected binary mixtures of mentioned components and measured eutectic temperatures (PDF)

■ AUTHOR INFORMATION

Corresponding Author

Remco Tuinier − *Laboratory of Physical Chemistry, Department of Chemical Engineering and Chemistry and Institute for Complex Molecular Systems, Eindhoven University of Technology, 5600 MB Eindhoven, The Netherlands;* orcid.org/0000-0002-4096-7107; Email: r.tuinier@tue.nl

Authors

Laura J. B. M. Kollau − *Laboratory of Physical Chemistry, Department of Chemical Engineering and Chemistry and Institute for Complex Molecular Systems, Eindhoven University of Technology, 5600 MB Eindhoven, The Netherlands; Laboratoire de Chimie, École Normale Supérieure de Lyon & CNRS, 69007 Lyon, France*

Job Verhaak − *Laboratory of Physical Chemistry, Department of Chemical Engineering and Chemistry, Eindhoven University of Technology, 5600 MB Eindhoven, The Netherlands*

Jaap den Doelder − *Laboratory of Physical Chemistry, Department of Chemical Engineering and Chemistry, Eindhoven University of Technology, 5600 MB Eindhoven, The Netherlands; Packaging and Specialty Plastics R&D, Dow Benelux BV, 4530AA Terneuzen, The Netherlands*

Ivo A. W. Filot − *Laboratory of Inorganic Materials and Catalysis, Department of Chemical Engineering and Chemistry and Institute for Complex Molecular Systems, Eindhoven University of Technology, Eindhoven, The Netherlands;* orcid.org/0000-0003-1403-8379

Mark Vis − *Laboratory of Physical Chemistry, Department of Chemical Engineering and Chemistry and Institute for Complex Molecular Systems, Eindhoven University of Technology, 5600 MB Eindhoven, The Netherlands;* orcid.org/0000-0002-2992-1175

Complete contact information is available at: https://pubs.acs.org/10.1021/acs.jpcb.0c01680

Notes

The authors declare no competing financial interest.

■ ACKNOWLEDGMENTS

We thank Dr. Catarina Esteves for useful discussions and advice on measuring the phase diagrams reported in this work. The members of the ISPT project 'Deep Eutectic Solvents in the pulp and paper industry' are thanked for their financial and

kind contributions. This cluster consists of the following organizations: Altri−Celbi, Buckman, Crown Van Gelder, CTP, DS Smith Paper, ESKA, Essity, Holmen, ISPT, Mayr−Melnhof Eerbeek, MetsäFibre, Mid Sweden University, Mondi, Omya, Parenco BV, The Navigator Company, Sappi, Essity, Smurfit Kappa, Stora Enso, Eindhoven University of Technology, University of Aveiro, University of Twente, UPM, Valmet Technologies Oy, Voith Paper, VTT Technical Research Centre of Finland Ltd, WEPA, and Zellstoff Pöls. Furthermore, this project received funding from the Bio-Based Industries Joint Undertaking under the European Union's Horizon 2020 research and innovation programme, under grant agreement no. 668970. M.V. acknowledges The Netherlands Organisation for Scientific Research (NWO) for a Veni grant (no. 722.017.005).

REFERENCES

(1) Abbott, A. P.; Capper, G.; Davies, D. L.; Rasheed, R. K.; Tambyrajah, V. Novel solvent properties of choline chloride/urea mixtures. *Chem. Commun.* **2003**, 70−71.
(2) Craveiro, R.; Aroso, I.; Flammia, V.; Carvalho, T.; Viciosa, M. T.; Dionísio, M.; Barreiros, S.; Reis, R. L.; Duarte, A. R. C.; Paiva, A. Properties and thermal behavior of natural deep eutectic solvents. *J. Mol. Liq.* **2016**, *215*, 534.
(3) Yusof, R.; Abdulmalek, E.; Sirat, K.; Rahman, M. B. A. Tetrabutylammonium bromide (TBABr)-based deep eutectic solvents (DESs) and their physical properties. *Molecules* **2014**, *19*, 8011.
(4) Dai, Y.; Witkamp, G. J.; Verpoorte, R.; Choi, Y. H. Tailoring properties of natural deep eutectic solvents with water to facilitate their applications. *Food Chem.* **2015**, *187*, 14.
(5) Florindo, C.; Oliveira, F. S.; Rebelo, L. P. N.; Fernandes, A. M.; Marrucho, I. M. Insights into the synthesis and properties of deep eutectic solvents based on choline chloride and carboxylic acids. *ACS Sustainable Chem. Eng.* **2014**, *2*, 2416−2425.
(6) Hayyan, A.; Mjalli, F. S.; Alnashef, I. M.; Al-Wahaibi, T.; Al-Wahaibi, Y. M.; Hashim, M. A. Fruit sugar-based deep eutectic solvents and their physical properties. *Thermochim. Acta* **2012**, *541*, 70−75.
(7) Hayyan, A.; Mjalli, F. S.; Alnashef, I. M.; Al-Wahaibi, Y. M.; Al-Wahaibi, T.; Hashim, M. A. Glucose-based deep eutectic solvents: Physical properties. *J. Mol. Liq.* **2013**, *178*, 137−141.
(8) Abranches, D. O.; Schaeffer, N.; Silva, L. P.; Martins, M. A.; Pinho, S. P.; Coutinho, J. A. The role of charge transfer in the formation of type i deep eutectic solvent-analogous ionic liquid mixtures. *Molecules* **2019**, *24*, 3687.
(9) Pontes, P. V.; Crespo, E. A.; Martins, M. A.; Silva, L. P.; Neves, C. M.; Maximo, G. J.; Hubinger, M. D.; Batista, E. A.; Pinho, S. P.; Coutinho, G.; João, A.; et al. Measurement and PC-SAFT modeling of solid-liquid equilibrium of deep eutectic solvents of quaternary ammonium chlorides and carboxylic acids. et al. *Fluid Phase Equilib.* **2017**, *448*, 69−80.
(10) Kollau, L. J. B. M.; Vis, M.; van den Bruinhorst, A.; Tuinier, R.; de With, G. Entropy models for the description of the solid−liquid regime of deep eutectic solutions. *J. Mol. Liq.* **2020**, *302*, 112155.
(11) Alhadid, A.; Mokrushina, L.; Minceva, M. Modeling of solid−liquid equilibria in deep eutectic solvents: A parameter study. *Molecules* **2019**, *24*, 2334.
(12) Abranches, D. O.; Martins, M. A. R.; Silva, L. P.; Schaeffer, N.; Pinho, S. P.; Coutinho, J. A. P. Phenolic hydrogen bond donors in the formation of non-ionic deep eutectic solvents: the quest for type V DES. *Chem. Commun.* **2019**, *55*, 10253−10256.
(13) García, G.; Atilhan, M.; Aparicio, S. An approach for the rationalization of melting temperature for deep eutectic solvents from DFT. *Chem. Phys. Lett.* **2015**, *634*, 151−155.
(14) Niedermeyer, H.; Ashworth, C.; Brandt, A.; Welton, T.; Hunt, P. A. A step towards the a priori design of ionic liquids. *Phys. Chem. Chem. Phys.* **2013**, *15*, 11566−11578.
(15) Hildebrand, J. H.; Scott, R. L. *The Solubility of Non-Electrolytes*, 3rd ed.; Rheinhold: New York, 1949.
(16) Hildebrand, J. The term regular solution. *Nature* **1951**, *168*, 868.
(17) Kollau, L. J. B. M.; Vis, M.; van den Bruinhorst, A.; Esteves, A. C. C.; Tuinier, R. Quantification of the liquid window of Deep Eutectic Solvents. *Chem. Commun.* **2018**, *54*, 13351.
(18) Margules, M. Über die Zusammensetzung der gesättigten Dämpfe von Misschungen. *Sitzungsberichte der Kaiserliche Akadamie der Wissenschaften Wien Mathematisch-Naturwissenschaftliche Klasse II* **1895**, *104*, 1243−1278.
(19) Venkatram, S.; Kim, C.; Chandrasekaran, A.; Ramprasad, R. Critical Assessment of the Hildebrand and Hansen Solubility Parameters for Polymers. *J. Chem. Inf. Model.* **2019**, *59*, 4188−4194.
(20) Kollau, L. J. B. M.; Vis, M.; van den Bruinhorst, A.; de With, G.; Tuinier, R. Activity modelling of the solid−liquid equilibrium of deep eutectic solvents. *Pure Appl. Chem.* **2019**, *91*, 1341−1349.
(21) Krooshof, G. J.; Tuinier, R.; de With, G. On the calculation of nearest neighbors in activity coefficient models. *Fluid Phase Equilib.* **2018**, *465*, 10.
(22) Staverman, A. J. The Entropy of High Polymer Solutions. *Recl. Trav. Chim. Pays-Bas* **1950**, *69*, 163−174.
(23) Guggenheim, E. A. Statistical thermodynamics of co-operative systems (a generalization o f the quasi-chemical method). *Trans. Faraday Soc.* **1948**, *44*, 1007−1012.
(24) Guggenheim, E. A.; McGlashan, M. L. Statistical mechanics of regular mixtures. *Proc. R. Soc. London, Ser. A* **1951**, *206*, 335−353.
(25) Rodriguez Rodriguez, N.; van den Bruinhorst, A.; Kollau, L. J. B. M.; Kroon, M. C.; Binnemans, K. Degradation of deep−eutectic solvents based on choline chloride and carboxylic acids. *ACS Sustainable Chem. Eng.* **2019**, *7*, 11521−11528.
(26) Zhang, H.; Xie, C.; Liu, Z.; Gong, J.; Bao, Y.; Zhang, M.; Hao, H.; Hou, B.; Yin, Q.-x. Identification and molecular understanding of the odd−even effect of dicarboxylic acids aqueous solubility. *Ind. Eng. Chem. Res.* **2013**, *52*, 18458−18465.
(27) Thalladi, V. R.; Nüsse, M.; Boese, R. The melting point alternation in α, ω-alkanedicarboxylic acids. *J. Am. Chem. Soc.* **2000**, *122*, 9227−9236.
(28) Acree, W. E. Thermodynamic properties of organic compounds: enthalpy of fusion and melting point temperature compilation. *Thermochim. Acta* **1991**, *189*, 37−56.
(29) Diarce, G.; Gandarias, I.; Campos-Celador, Á.; García-Romero, A.; Griesser, U. J. Eutectic mixtures of sugar alcohols for thermal energy storage in the 50−90 °C temperature range. *Sol. Energy Mater. Sol. Cells* **2015**, *134*, 215−226.
(30) Coker, T. G.; Ambrose, J.; Janz, G. J. Fusion properties of some ionic quaternary ammonium compounds. *J. Am. Chem. Soc.* **1970**, *92*, 5293−5297.
(31) Kollau, L. J. B. M. On the quantification, description, and prediction of eutectic mixtures. Ph.D. Thesis, Eindhoven University of Technology, 2019; https://pure.tue.nl/ws/portalfiles/portal/127273627/20190522_CO_Kollau.pdf.
(32) Elstner, M.; Hobza, P.; Frauenheim, T.; Suhai, S.; Kaxiras, E. Hydrogen bonding and stacking interactions of nucleic acid base pairs: A density functional-theory based treatment. *J. Chem. Phys.* **2001**, *114*, 5149−5155.
(33) Béguin, C.; Gäumann, T. Das dipolmoment der Dicarbonsäuren. *Helv. Chim. Acta* **1958**, *41*, 1376−1386.
(34) Girard, P. Dipole association in pure liquids. *Trans. Faraday Soc.* **1934**, *30*, 763−772.
(35) Brönsted, J. N. Einige Bemerkungen über den Begriff der Säuren und Basen. *Recl. des Trav. Chim. des Pays-Bas* **1923**, *42*, 718−728.
(36) Lowry, T. M. The uniqueness of hydrogen. *J. Soc. Chem. Ind., London* **1923**, *42*, 43−47.
(37) Gilli, G.; Gilli, P. Towards an unified hydrogen-bond theory. *J. Mol. Struct.* **2000**, *552*, 1−15.

https://dx.doi.org/10.1021/acs.jpcb.0c01680
J. Phys. Chem. B 2020, 124, 5209−5219

(38) Lindvig, T.; Michelsen, M. L.; Kontogeorgis, G. M. A Flory-Huggins model based on the Hansen solubility parameters. *Fluid Phase Equilib.* **2002**, *203*, 247−260.
(39) Stefanis, E.; Panayiotou, C. Prediction of Hansen solubility parameters with a new group-contribution method. *Int. J. Thermophys.* **2008**, *29*, 568−585.
(40) Abdi, H.; Williams, L. J. Principal component analysis. *WIREs Comput. Stat.* **2010**, *2*, 433−459.
(41) Wold, S.; Esbensen, K.; Geladi, P. Principal component analysis. *Chemom. Intell. Lab. Syst.* **1987**, *2*, 37−52.
(42) Kresse, G.; Hafner, J. Ab initio molecular dynamics for liquid metals. *Phys. Rev. B: Condens. Matter Mater. Phys.* **1993**, *47*, 558−561.
(43) Kresse, G.; Hafner, J. Ab initio molecular-dynamics simulation of the liquid-metalamorphous- semiconductor transition in germanium. *Phys. Rev. B: Condens. Matter Mater. Phys.* **1994**, *49*, 14251−14269.
(44) Kresse, G.; Furthmüller, J. Efficiency of ab-initio total energy calculations for metals and semiconductors using a plane-wave basis set. *Comput. Mater. Sci.* **1996**, *6*, 15−50.
(45) Kresse, G.; Furthmüller, J. Efficient iterative schemes for ab initio total-energy calculations using a plane-wave basis set. *Phys. Rev. B: Condens. Matter Mater. Phys.* **1996**, *54*, 11169−11186.
(46) Perdew, J. P.; Burke, K.; Ernzerhof, M. Generalized gradient approximation made simple. *Phys. Rev. Lett.* **1996**, *77*, 3865−3868.

https://dx.doi.org/10.1021/acs.jpcb.0c01680
J. Phys. Chem. B 2020, 124, 5209−5219